NASA
Technical Memorandum 87073
AIAA-85-1133

USAAVSCOM
Technical Report 85-C-8

Rotor Wake Characteristics of a Transonic Axial Flow Fan

M.D. Hathaway
Propulsion Directorate
U.S. Army Aviation Research and Technology Activity—AVSCOM
Lewis Research Center
Cleveland, Ohio

J. Gertz and A. Epstein
Massachusetts Institute of Technology
Cambridge, Massachusetts

and

A.J. Strazisar
Lewis Research Center
Cleveland, Ohio

NASA

ROTOR WAKE CHARACTERISTICS OF A TRANSONIC AXIAL FLOW FAN

M. D. Hathaway[*]
U.S. Army Propulsion Directorate (AVSCOM), Cleveland, Ohio

J. Gertz[**] and A. Epstein[†]
Massachusetts Institute of Technology, Cambridge, MA

and

A. J. Strazisar[††]
NASA Lewis Research Center, Cleveland, Ohio

Abstract

State of the art turbomachinery flow analysis codes are not capable of predicting the viscous flow features within turbomachinery blade wakes. Until efficient 3D viscous flow analysis codes become a reality there is therefore a need for models which can describe the generation and transport of blade wakes and the mixing process within the wake. To address the need for experimental data to support the development of such models, high response pressure measurements and laser anemometer velocity measurements have been obtained in the wake of a transonic axial flow fan rotor.

Nomenclature

a	longitudinal spacing of the vortices
C	Chen's Universal Wake Number
C_p	static pressure coefficient (see Eq. (11))
h	lateral spacing of the two rows of vortices in a vortex street
k	strength of a vortex
P	static pressure
q'	velocity in the vortex street in the (x',y') frame moving with the vortices
q_{rel}	velocity in the vortex street in the (x,y) frame fixed to the rotor blade trailing edge
q_o	velocity at the edge of a vortex core
r_o	radius of a vortex core
u	velocity component in the direction parallel to the motion of the vortex street
U_i	velocity induced by the vortex street (see Eq. (5))
U_s	velocity of the vortex street (see Eq. (6))
U_∞	equivalent free-stream velocity of the vortex street in the frame fixed to the rotor blades
v	velocity component in the direction perpendicular to the motion of the vortex street
w	complex velocity of a single infinite row of vortices (see Eq. (1))
W	wake width
x	coordinate in the direction of motion of the vortex street
y	coordinate perpendicular to the motion of the vortex street
β_{av}	pitchwise-averaged flow angle measured by the LA
β_{rel}	pitchwise-averaged flow angle in the frame moving with the rotor blades (also the direction of motion of the vortex street)
ρ_∞	free-stream static density

Superscripts

(')	denotes the frame of reference moving with the vortex cores with its origin along the centerline of the vortex street
(")	denotes a frame of reference moving with the vortex cores with its origin at the center of a vortex core in either the upper or lower row of vortices

Subscripts

core	denotes an isolated vortex core
pot	denotes an isolated potential vortex
row	denotes a row of potential vortices
∞	denotes the equivalent free-stream of the rotor blade vortex street
upper	denotes upper row of vortices with negative circulation
lower	denotes lower row of vortices with positive circulation

Introduction

Over the past several years, the MIT Gas Turbine Laboratory and the NASA Lewis Research Center have been investigating the flowfields upstream, within, and downstream of transonic compressor blade rows in order to provide data for the validation of numerical analysis methods and to improve our understanding of the flow phenomena which govern transonic compressor performance. MIT has used high frequency response probes outside the blade row to measure time resolved blade-to-blade distributions of total and static pressure, flow angle, and total temperature of the same transonic fan stage in both a conventional single-stage compressor test facility at NASA Lewis and in the MIT Blowdown Compressor Test Facility. NASA Lewis has used laser anemometry within and outside the blade row to measure blade-to-blade distributions of velocity and flow angle in the Lewis compressor test facility.

One of the flow phenomena being investigated during this effort is that of the unsteady character of the rotor wakes and its effect on wake mixing. The rotor wakes in this machine will be shown to consist of highly-structured vortex streets, similar in many respects to the unsteady flowfields observed behind bluff bodies as a result of classical Von-Karman vortex shedding. This phenomena is of interest to the designer since it is a source of total pressure loss, flow unsteadiness, and acoustic excitation. It is important to the analyst since it cannot be accounted for by three-dimensional inviscid flowfield prediction techniques and is incompatible with techniques which assume steady flow boundary conditions. The

[*]Aerospace Engineer
[**]Research Assistant
[†]Assistant Director, Gas Turbine Laboratory
[††]Head, Aerodynamics Section

extent to which the wake is not completely mixed out between blade rows results in an error in the numerical predictions for multiple blade rows due to unsteady effects. Therefore, until efficient, unsteady, fully-viscous flowfield predictions become available, an empirical data base is required for use in creating models for the development and transport of blade wakes.

Vortex streets have been well documented in the wakes behind bluff bodies, flat plates, and airfoils with blunt trailing edges, both isolated and in cascade. They have been observed through the transonic regime and at Reynolds numbers typical of gas turbine operation. Techniques used include high speed flow visualization [1],[2],[3], spectral analysis of hot wire signals [4], and probability density measurements from laser anemometers [5]. Studies of the shedding from airfoils with sharp trailing edges typical of fan and compressor blading are somewhat ambiguous, some showing shedding, some not [6].

In this paper, we will present experimental evidence supporting the existence of a vortex street structure in the rotor blade wake, develop a simple model of the wake structure which fits the data, and discuss some of the implications of this structure to compressor performance and analysis.

Experimental Apparatus

Test Compressor

The research compressor used in the present study was the first stage of a NASA Lewis designed, two-stage axial flow fan [7]. The first-stage rotor was designed as a low aspect ratio (1.56) damperless fan with a design pressure ratio of 1.63 at a massflow of 33.25 kg/sec. The design rotational speed is 16,000 rpm, which yields a design tip speed of 429 m/sec. The inlet relative Mach number at the rotor tip is 1.38. The first-stage rotor has 22 blades, an inlet tip diameter of 51.3 cm, and an inlet hub/tip radius ratio of 0.375. The rotor tip clearance at design speed is 0.5 mm.

The rotor was tested in the present study in several configurations: as an isolated rotor, with a 34 blade multiple-circular-arc (MCA) designed stator row (see [7]), and with a 17 blade controlled diffusion (CD) designed stator row. The experimental investigation presented herein was prompted from the analysis of data gathered during tests of the isolated rotor and with the 34-blade MCA stator. Further investigations of the rotor flow-field features presented in this paper were completed with the 17-blade CD stator present. The stator blade rows were located approximately 80% of rotor chord downstream of the rotor trailing edge at midspan. The upstream influence of the stator on the rotor flowfield was found to extend no closer than 50% of rotor chord downstream of the rotor trailing edge, as determined from observing the axial location at which circumferential variations in the absolute velocity were no longer discernible to the laser anemometer. Hereafter, no mention of the particular configuration for which the results were obtained will be given as the rotor flowfield phenomena discussed herein was independent of the configuration tested.

Laser Anemometer System

The laser anemometer system used in the present experimental investigation is a single channel, dual beam, fringe anemometer with on-axis back-scatter collection optics, and has been previously described in detail [8],[9]. Optical access to the compressor flowfield is provided through a 3mm thick glass window which closely conforms to the rotor flowpath contour in both the circumferential and streamwise directions, thus minimizing the disturbance of the tip region flow.

Flourescent liquid seed particles, nominally 1-1.4 microns in diameter, are introduced into the flowfield through a 6 mm diameter tube located 35 mm upstream of the rotor. The seeder tube is installed in a radial and circumferential actuator to provide capability for positioning the seeder to optimize the data rate each time the laser probe volume location is changed.

Each time an LA velocity measurement is acquired, it is tagged with the rotor rotational position at which it occurred. This position information is used to assign the velocity measurement to the proper circumferential location relative to the rotor blade. Measurements are acquired across 17 of the 22 rotor blade passages, but are averaged into one representative blade passage containing 50 equally spaced blade-to-blade measurement locations. The individual velocity measurements which occur at each blade-to-blade measurement location are sorted into "velocity bins" which are 1.5 m/sec wide. This process yields a probability density distribution (p.d.d.) for the measured velocity at each of the 50 blade-to-blade measurement locations. The mean velocity at each measurement location is the mean of the corresponding p.d.d. The p.d.d.'s and corresponding mean velocity distribution across approximately one-half of a rotor blade pitch are shown in Fig. 1. The solid line is a curve fit through the mean velocity of each p.d.d. For the sake of clarity, the height of each p.d.d. in Fig. 1 has been normalized by the height of its highest bin.

High Frequency Response Probe

Time-resolved blade-to-blade measurements of total and static pressure, as well as radial and tangential flow angle, were obtained using a 4-sensor cylinder-type probe developed at MIT [10]. The probe actually has a 3.3 mm elliptical cross-section with four high-response silicon diaphragm pressure transducers flush mounted on the surface. The frequency response of the probe is limited by the probe size to between 10 and 20 kHz [11].

A high speed pneumatic translator traversed the probe across the blade span to a fixed radial position where it was held for appoximately 0.5 sec and then withdrawn into a small calibration chamber outside the casing wall which was sealed by a quick opening (20 ms) gate valve. The chamber was connected to an external pressure reference system so that the sensors could be calibrated before and after each immersion. The analog pressure signals and a once-per-rev signal were recorded on an FM tape recorder and later played back and digitized at an equivalent real-time sampling rate of 200 kHz per channel, resulting in 30 to 40 data points sampled per blade passing.

The pressure signals were reduced to instantaneous total and static pressure (and thus Mach number) and two flow angles using calibration curves [12]. The total temperature was then calculated using the Euler turbine equation.

Experimental Findings

Previous analyses of laser anemometer measurements presented in [4] and [13] indicate that the presence of moving vortices is clearly manifested in LA measurements by the existence of a bi-modal velocity probability distribution (p.d.d.). In order to further investigate the possibility of vortex shedding in the rotor blade wake, simultaneous LA/ellipse probe experiments were conducted in the NASA Lewis compressor test facility.

At each radius investigated, an LA run was made at the pitchwise-averaged flow angle, β_{av}, determined from earlier LA measurements. Figure 2 is the mean velocity distribution measured during an LA run made at the rotor exit aero-survey station at 60% span, 140% chord at an angle, β_{av}, of 42 degrees. The mean velocity distribution is obtained by averaging together the velocity distributions in each of the 17 measured blade passages. The probability density distributions of the measurements at points labelled A through F in Fig. 2 are shown in Fig. 3. In each case the abscissa is the number of velocity measurements which occurred within a velocity "bin" which is 1.5 m/sec wide. The ordinate is the center velocity of each "bin". Also shown on the ordinate scale is the mean velocity determined from each p.d.d. These mean velocities form the time-averaged velocity distribution of Fig. 2. In the core flow region outside of the wake (points A and F), the p.d.d. is single-valued. The most probable velocity always occurs in the bin centered at 235 m/sec. In the edges of the wake (points B and E), the probability of velocities in the range of 180-200 m/sec begins to rise. At the center of the wake (points C and D), the probability of velocities centered at these low levels reaches a maximum. However, a significant number of velocity measurements still occur at the free stream level of 235 m/sec.

Measurements of the instantaneous velocity and flow angle were acquired by the ellipse probe at the same axial station as the LA. The instantaneous relative flow angle determined by the ellipse probe measurements is shown in the upper trace of Fig. 4, while a 90 rotor revolution ensemble average is shown below it. The ensemble averaged data is quite similar to that from the LA with the relatively small blade-to-blade variations probably attributable to geometric differences. The instantaneous measurement, however, shows enormous angle swings in the wake. Similar variations can be seen in measurements of total and static pressure. Swings of this magnitude are likely to result from the probe measuring an approximately instantaneous snapshot of the periodic vortex sheet in the wake as it is convected past the stationary probe.

The probe data has been analyzed to derive velocity probability distributions corresponding to those from the LA data. For purposes of this comparison, the location of the blade wake measured by the probe is obtained by examining the time trace of the velocity component which lies 42 degrees from the axial direction (i.e., the velocity component measured by the LA). The probe signal

for a time period of slightly more than one blade passing time is shown in Fig. 5. The upper trace is the instantaneous velocity distribution across blade passage #1, which is defined as the first blade passage which occurs after passage of the once-per-rev timing reference mark on the rotor disk. The lower trace is a rotor-averaged velocity distribution across blade passage #1, which is calculated by averaging the instantaneous distributions measured during 90 consecutive rotor revolutions. Points labelled A-F correspond to similarly labelled points in the LA data of Fig. 2. These points have been located on the probe data by setting point C at the bottom of the wake and locating the remaining points at the proper pitchwise location relative to point C. Probability density distributions can now be formed for the probe data by considering the digitized data which occurs at points A-F. Performing this process on data acquired during 90 consecutive rotor revolutions yields the p.d.d.'s shown in Fig. 6 for rotor blade passage #1. Due to the lower spatial resolution of the ellipse probe, the p.d.d. at the wake centerline does not clearly have a bimodal distribution like the LA p.d.d.. However, there is a wider range of velocities which occur in the wake than in the coreflow. The p.d.d.'s at pitchwise locations within the wake show a gradual increase in the width of the p.d.d. as one moves from the wake edges toward the center of the wake.

In order to further investigate the nature of the flow in the wake, each LA bimodal p.d.d. acquired in the blade wake was partitioned into a high velocity and a low velocity portion as shown in Fig. 7, for example. The mean velocity of each single-moded p.d.d. was then calculated, and is plotted at each measurement location across the blade wake in Fig. 8. The solid curve in Fig. 8 is the time-mean velocity distribution shown in Fig. 2, while the broken lines are the mean velocities calculated from the partitioned segments of the p.d.d.'s in the wake. These results indicate that the wake is not formed by the mixing of two shear layers but is rather the time average of two different velocity states. One of these velocity states is centered near the core flow velocity level while the other state is lower than the core flow level by nearly twice the time-mean wake velocity deficit. In addition, the p.d.d.'s at points C and D indicate that the flow at points near the wake centerline actually spends little time at the time-averaged velocity level.

Rotor-Blade Wake Model

It is proposed that the rotor blade wakes be modeled as modified ideal Karman vortex streets consisting of two staggered rectilinear rows of Rankine vortices of opposite sign in a uniform free stream. The analysis is performed in the reference frame moving with the vortex cores, and a coordinate transformation is used to compute the flowfield as would be seen by a stationary probe.

The vortex street is modeled by summing the contributions of the two staggered rows of Rankine vortices. Each vortex consists of an inner and outer region, the boundary of which is denoted as the core radius, r_0. The inner region consists of forced-vortex flow while the outer region follows the irrotational flowfield of a classical VonKarman vortex street of point vortices. The addition of

finite vortex cores is considered a more realistic assumption, since it avoids infinite velocities at the vortex centers and also allows for smoothly varying averaged wake profiles, as seen in the experimental data. Following Lamb [14], the complex velocity of a single infinite row of equally spaced vortices of strength, k, and spaced a distance, a, can be written as

$$w(z) = u'' - iv'' = \frac{-ik}{2a} \cot \frac{\pi z}{a} \tag{1}$$

where, $z = x'' + iy''$ as shown in Fig. 9a. Here the (x'', y'') frame moves with the vortex cores and is fixed to the center of a vortex in either the upper or lower row. In this frame, the velocity components parallel and perpendicular to the direction of motion of the vortices are u'' and v'' respectively. The (x', y') frame also moves with the vortex cores but is positioned at the center-line between the two rows of vortices. A third reference frame, (x, y), is fixed to the rotor blade trailing edge. The velocity components in the (x', y') and (x, y) frames are (u', v') and (u, v) respectively.

These components will be non-dimensionalized with respect to the pressure-defect velocity, U_p, which represents the velocity at the edge of an isolated vortex core and is related to the pressure drop from the free-stream to the edge of an isolated core.

$$U_p = \frac{k}{2\pi r_0} \tag{2}$$

All lengths will be expressed with respect to the vortex spacing, a, and the equations describing the velocity components of a single isolated row in the (x'', y'') frame are then,

$$\bar{u}'' = -\bar{k} \frac{\sinh 2\pi \bar{y}''}{\cosh 2\pi \bar{y}'' - \cos 2\pi \bar{x}''} \tag{3a}$$

and,

$$\bar{v}'' = \bar{k} \frac{\sin(2\pi \bar{x}'')}{\cosh 2\pi \bar{y}'' - \cos 2\pi \bar{x}''} \tag{3b}$$

where,

$$\bar{u}'' = \frac{u}{U_p}, \qquad \bar{v}'' = \frac{v}{U_p}$$

$$\bar{x}'' = \frac{x''}{a}, \qquad \bar{y}'' = \frac{y''}{a}$$

$$\bar{k} = \frac{k}{2aU_p}$$

To ensure that the velocity decays smoothly from the edge to the center of the vortex core, the velocity in the vortex core is obtained by subtracting the contributions of an isolated potential vortex from the velocity field of the row of vortices and adding the contributions of an isolated viscous core. The velocity components in a vortex core of positive circulation (lower row) are then,

$$\bar{u}'' = [\bar{u}_{row} - \bar{u}_{pot}] + \bar{u}_{core} \tag{4a}$$

$$\bar{v}'' = [\bar{v}_{row} - \bar{v}_{pot}] + \bar{v}_{core} \tag{4b}$$

where,

$$\bar{u}_{pot} = -\left(\frac{r_0}{r}\right)\left(\frac{\bar{y}''}{\bar{r}}\right) \qquad \bar{u}_{core} = -\left(\frac{\bar{y}''}{\bar{r}_0}\right)$$

$$\bar{v}_{pot} = \left(\frac{r_0}{r}\right)\left(\frac{(\bar{x}'')_{min}}{\bar{r}}\right) \qquad \bar{v}_{core} = \left(\frac{(\bar{x}'')_{min}}{\bar{r}_0}\right)$$

Here $(\bar{x}'')_{min}$ is the axial distance to the center of the nearest vortex core. For a vortex core of negative circulation (upper row), the direction of the contributions due to the isolated vortex must be reversed.

The flowfield of the complete vortex street is now found by summing the velocity components of two isolated rows spaced h apart and staggered by a/2. Each row induces a motion in the opposite row which results in motion of the entire vortex street. This motion, the induced velocity, U_i, is found by solving for the velocity induced at the center of a vortex by the opposing row.

$$U_i = \frac{-k}{2a} \tanh\left(\pi \frac{h}{a}\right) \tag{5}$$

If the vortex street is formed in a free-stream of velocity, U_∞, then in the frame of reference fixed to the blades (x, y) the vortex-street moves with velocity, U_s, where,

$$U_s = U_\infty + U_i \tag{6}$$

In the (x', y') frames, the free-stream velocity is simply $(-U_i)$. The velocity components in the primed frame are then,

$$u' = u_{upper} + u_{lower} - U_i \tag{7a}$$

$$v' = v_{upper} + v_{lower} \tag{7b}$$

The velocity, q', is then,

$$q' = \sqrt{(u')^2 + (v')^2} \tag{8}$$

Given a location in the (x', y') frame, the upper and lower velocity components can be calculated from Eqs. (3a) and (3b) by a simple coordinate transformation. For the upper row,

$$\bar{x}'' = \bar{x}' - 1/2 \qquad \bar{y}'' = \bar{y}' - h/2a$$

and for the lower row,

$$\bar{x}'' = \bar{x}' \qquad \bar{y}'' = \bar{y}' + h/2a$$

Since the vortex cores move at a velocity of $(U_\infty + U_i)$, the parallel and perpendicular velocity components in the frame relative to the rotor blades (x, y) are then,

$$u_{rel} = u' + (U_\infty + U_i) \tag{9a}$$

$$v_{rel} = v' \tag{9b}$$

The relative velocity is then,

$$q_{rel} = \sqrt{(u_{rel})^2 + (v_{rel})^2} \tag{10}$$

(Note: $(q_{rel})_\infty = U_\infty$.)

To facilitate the fit of the model to measurements, the velocity components predicted by the

4

vortex model are translated from the blade relative frame to the stationary laboratory frame in a straightforward coordinate transformation using the velocity triangle shown in Fig. 9b with the measured wheel speed (U) and average exit angle $(\beta_{rel})_\infty$.

Pressure Coefficient

In the frame of reference moving with the vortices (x',y'), the flow is steady and the free-stream velocity is equal to $(-U_i)$. For the cases considered here, it is sufficient to assume constant density, since the maximum Mach number in this frame of reference is approximately 0.10. In the irrotational, inviscid regions outside the vortex cores, the pressure, found simply from Bernoulli's equation, is expressed in terms of a pressure coefficient based on the pressure-defect velocity, U_p,

$$\bar{C}_p \equiv \frac{p - p_\infty}{\rho_\infty U_p^2} \qquad (11)$$

Thus, outside of a vortex core, $r \geq r_0$,

$$C_p = -\frac{1}{2}\left[(\bar{q}')^2 - \bar{u}_i^2\right] \qquad (12)$$

Within a vortex core, the radial momentum equation is integrated across the core. The inner and outer pressure solutions are matched at r_0 with the variation in velocity accounted for by the average of the velocity squared around the circumference. The pressure at the center of the vortex is then expressed in terms of this average velocity, $\langle q_0^2 \rangle$, and the pressure coefficient inside the vortex cores, $r < r_0$,

$$\bar{C}_p = -\frac{1}{2}\langle \bar{q}_0^2 \rangle \left[2 - \left(\frac{r}{r_0}\right)^2 \left(2 - \frac{\bar{q}_0^2}{\langle \bar{q}_0^2 \rangle}\right)\right] + \frac{\bar{u}_i^2}{2} \qquad (13)$$

The average of the velocity squared at the vortex core, $r=r_0$, can be found numerically given the vortex street geometry. For a typical Von-Karman-like street (h/a=0.28) $\langle q_0^2 \rangle$ is nearly equal to unity (1.002). For values of $r<r_0$, q_0, is evaluated at a point on the circumference ($r=r_0$) where a ray from the center of the vortex through the point in question intersects the edge of the core at $r=r_0$.

Fitting the Model to LA Data

The wake model described above is quite general. We now need to specify or set the parameters (geometry and vortex strength) to represent the transonic compressor flowfield. The geometry of the vortex street is specified by the lateral spacing ratio, h/a, and the core-radius ratio, r_0/h, while the strength of the vortices is related to the ratio of the pressure-defect velocity to the free-stream velocity, U_p/U_∞.

Little in the way of quantitative data concerning the parameters which characterize the vortex street is available in the literature for geometries other than right circular cylinders. A comprehensive overview of the available data for vortex shedding on circular cylinders has been presented by Chen [15] for a wide range of Reynold's numbers (based on the cylinder diameter) up to 10^7. He uses a "universal wake number", shown to be valid over the entire range of Reynolds numbers, essentially

$$C = \frac{\left(\frac{h}{a}\right)^2}{2}\left[\frac{1}{\pi \frac{h}{a}(r_0/h)(U_p/U_\infty)} - \tanh\pi\frac{h}{a}\right] \qquad (14)$$

Chen found the value of the constant, C, to be 0.172 for highly turbulent flows and 0.165 for flows with low free-stream turbulence. As will be shown, a considerably larger value is obtained for the rotor blade wakes investigated here.

The experimental data for the vortex spacing ratio, h/a, in flows behind circular cylinders, show a large spread with respect to Karman's stability criteria of 0.2806. Good correlations are not available in the literature at high Reynold's numbers [16]. Low Re data ranges from 0.06 to 0.31 [17],[18].

Without "classical" experimental data as a guide, the vortex street model was fit to the laser anemometer data. The core-radius ratio, r_0/h, and vortex strength, k, were chosen so as to match certain features of the average wake profile as measured by the LA. The spacing ratio was then chosen such that the probability density distribution of the velocity at the wake centerline approximates the bi-modal distribution measured by the LA. This was accomplished by matching both the upper and lower most-probable velocities.

The core-radius is chosen so that the averaged velocity profile of the vortex street resembles a smooth wake-like profile of the type observed in both the LA and 4-way probe data. If the core-radius is considerably smaller than the spacing between the two rows of vortices ($r_0/h \ll 1$), then the averaged velocity profile across the wake will have a uniform defect. In order to match the averaged experimental velocity profiles, the core-radius, r_0, must be at least one-half the vortex spacing, h. This corresponds to a vortex street in which the edge of the vortex cores on both the upper and lower rows of the street coincide with the wake centerline. Schaefer and Eskinazi [16] reported core-radius ratios of between 0.50 and 0.86 in what is described as a stable region of "periodic regularity" behind the cylinder. For purposes of this study, a core-radius ratio of 0.5 is used.

The actual wake size, W, is determined by the extent of the vortex cores and can be expressed as a function of the vortex spacing, h, and the core radius, r_0.

$$W = h[1 + 2(r_0/h)] \qquad (15)$$

For r_0/h equal to 0.5, h is exactly one-half the wake width.

The vortex strength as represented by the quantity, $k/(2\pi a U_\infty)$, will determine the depth of the averaged "measured" velocity profile. A velocity profile calculated with a vortex strength of 0.07 is shown in Fig. 10 where it is compared to the experimentally measured profile. For purposes of this comparison, the actual vortex spacing, h, has been set so that the width of the wake predicted by the model matches the measured wake width, which in this case is approximately 26 percent of the blade passage.

From the LA p.d.d. for the wake centerlines (see Fig. 3, point C), the two most probable velocities in the bi-modal distribution can be seen to be,

$$V_{high} = 238 \text{ m/sec}, \quad V_{low} = 192 \text{ m/sec}$$

These velocities can be calculated from the vortex wake model as a function of the vortex spacing ratio, h/a, by non-dimensionalizing the vortex street free-stream velocity, U_∞, which can be found from the rotor exit velocity triangle shown in Fig. 9b. Using a measured wheel speed of 281 m/sec, an average exit angle of 45°, and a measured absolute free-stream velocity of 235 m/sec, U_∞ is found to be equal to 202 m/sec. A vortex spacing ratio of 0.635 results in a good match of both the upper and lower most probable velocities for a vortex strength of 0.07.

Given the vortex strength, the core-radius ratio (r_o/h) and the spacing ratio (h/a), the pressure velocity, U_p, can be found since,

$$\frac{U_p}{U_\infty} = \frac{\dfrac{k}{2\pi a U_\infty}}{\left(\dfrac{r_o}{h}\right)\left(\dfrac{h}{a}\right)} \tag{16}$$

This results in a value of 0.22.

A summary of the parameters which determine the shape and strength of the rotor blade vortex street can be seen in Table 1 and a comparison of certain key measurements to the predictions of the model can be seen in Table 2. There is an excellent match of the values of the two most probable velocities even though the wake profile predicted by the model is not quite as deep as the measured profile.

Histograms of the probability density distribution, as would be measured by the laser anemometer in this vortex street, are shown in Fig. 11 for the points labelled on Fig. 12. Note the bimodal velocity distribution at the wake centerline (C) and compare with the measured distribution in Fig. 3.

Comparison of The Model to Probe Data

The predictions of the vortex model can now be compared with the time-resolved measurements made with the ellipse probe. Many of these comparisons will tend to be qualitative in nature since the probe's diameter is about half the size of the vortex core. Also, the probe calibrations used do not account for large gradient effects which may be present near the vortex cores. Additional information is required about the mean core flow in order to fully specify the rotor exit flowfield. This data was input from the steady state measurements and includes the ratio of freestream static pressure to rotor inlet total pressure (1.20), freestream absolute total temperature ratio (1.175), and freestream Mach number (0.59).

Vortex model time traces are calculated by sampling the flowfield predicted by the model in a manner which simulates the passage of the wake past the probe. The resulting time trace takes into account the rotor wheel speed and the convection of the vortices in the mean relative flow angle direction. Each sampling through the street constitutes a blade passing and begins at a random value of

(x'/a) between 0.0 and 1.0, and then proceeds through the street according to the probe's trajectory. The coordinates of the probe's position in the frame fixed to the vortices will then vary in time for each simulated blade passing.

The relative flow angle is compared in Fig. 12. The effect of the vortex structure is to add a pseudo-random component to what would otherwise be a periodic structure. This type of fluctuation then agrees with measurement, although the amplitude of the fluctuations are underpredicted, perhaps due to probe size limitations discussed above.

Total pressure is compared in Fig. 13. The model predicts both the pressure defects and excesses in the blade wake, as well as about the same amplitude of fluctuation. The agreement is not as close for the static pressure (Fig. 14). The probe shows much larger fluctuation than does the model. (The low static pressure spikes in the model results are the vortex cores, while the high static pressure peaks are the relatively low velocity regions between the vortices.) The trend is similar for other flow variables; the model predicts the nature of the perturbation about the mean but underpredicts the amplitude of the fluctuations.

Discussion

The simple vortex street wake model fits the experimental data reasonably well. The vortex model reproduces the wake shape and bimodal p.d.d., a feature otherwise difficult to explain. The vortex model also matches the high frequency response probe data. The high level of blade to blade variation, observed in several transonic rotors [10],[18], has always been puzzling since the level of fluctuation was always much higher than could be accounted for by geometric blade to blade differences. The intermittent sampling of the vortex street by the fixed frame probe reproduces these features, as shown in Figs. 12-14.

From the above, we conclude that a vortex street is present in the wake of the transonic compressor rotor. The flow is undoubtedly more complex than the simple model presented above. The time evolution of the vortex street must be considered, including the exact structure of the cores. The three-dimensional structure of the vorticity is also important since, if the vortex pattern has an appreciable spanwise coherence, radial fluid transport along the vortex cores can be considerable. This radial transport would appear as a spanwise redistribution of the wake flow, evolving in the streamwise direction. Thus, much work needs to be done on the structure of the vortex street.

The frequency of the vortex shedding can be calculated from the parameters of the model and the actual measured width of the wake, W, as follows,

$$f = \left(\frac{h}{a}\right)\left[1 + 2\left(\frac{r_o}{h}\right)\right]\left(\frac{U_\infty}{W}\right)\left(1 + \frac{U_i}{U_\infty}\right) \tag{17}$$

(Note: $U_i < 0$).

For the parameters in Table 1 and the measured wake width of 1.28 cm, the shedding frequency is calculated as 16 kHz. This frequency coincides with that measured in an earlier shock motion study [18]. This is an independent confirmation that the airfoil wake does indeed produce a disturbance at the frequency observed in the core flow and, thus, that the shedding may drive the shock system.

We believe that most, if not all, blades shed vortices in their wakes. This shedding, however, can be either strong and continuous or weak and intermittent. Experimental evidence [19] suggests that all bodies shed vortices but the shedding can be intermittent, i.e., the vortices are shed in bursts. Due to the lack of phase coherence between bursts, this fixed frequency but incoherent disturbance will not be readily detectable using simple spectral methods on signals from hot wires or microphones, but are apparent in instantaneous flow visualizations. Even when the shedding is continuous, its perturbation of the mean flow when viewed in the stationary frame can be quite small.

Recent work [20] has shown that vortex shedding from cylinders can lock on in frequency and phase to an external disturbance. The lock-on also has the effect of increasing the intensity of the shedding. This is similar to the acoustic resonance effects observed in both isolated airfoils and cascades [21],[22]. Phase locking has also been observed in a transonic cascade [23]. This implies that the same airfoil may shed weakly or strongly depending on its environment, behaving differently in a rotor versus cascade testing. The nature of the external disturbance may be acoustic resonance or a blade row interaction.

Conclusions

Our principal conclusion is that the transonic compressor rotor studied sheds a vortex street in the blade wakes. These vortices account for the bimodal velocity distribution observed by the laser anemometer and the large blade to blade fluctuations seen with the high frequency response instrumentation. The presence of the vortex street has several implications for the understanding of fan fluid physics, which are not presently accounted for in analysis or design.

Acknowledgements

The authors wish to acknowledge many useful conversations with Professor M. Kurosaka.

References

1. Davies, M.R.D. and Bryanston-Cross, P.J., "Holographic Measurements and Theoretical Predictions of Unsteady Flow in a Transonic Annular Cascade," J. Eng. for Power, Vol. 107, No. 2, 1985.

2. Heinemann, H.J. and Butefisch, K.A., "Determination of the Vortex Shedding Frequency of Cascades with Different Trailing Edge Thicknesses," AGARD CP-227, 1977, pp. 35-1 to 35-10.

3. Heinemann, H.J., Lawaczeck, O., Butefisch, K.A., "V. Karman Vortices and Their Frequency Determination in the Wakes of Profiles in the Sub- and Transonic Regimes," IUTAM Symposium, 1976, pp. 75-82.

4. Paterson, R.W. and Weingold, H.P., "Experimental Investigation of a Simulated Compressor Airfoil Trailing Edge Flowfield," AIAA-84-0101, 1984.

5. Dunker, R.J., "Flow Measurements in the Stator Row of a Single Stage Transonic Axial Compressor with Controlled Diffusion Stator Blades," AGARD CP-351, 1983.

6. Hobbs, D.E., et al., "Experimental Investigation of Compressor Cascade Wakes," ASME 82-GT-299, April 1982.

7. Urasek, D.C., Gorell, W.T., and Cunnan, W.S., "Performance of Two-Stage Fan Having Low-Aspect-Ratio, First-Stage Rotor Blading," NASA TP-1493, August 1979.

8. Strazisar, A.J., Powell, J.A., "Laser Anemometer Measurements in a Transonic Axial Flow Compressor Rotor," ASME Journal of Engineering for Power, Vol. 103, No. 2, April 1981.

9. Powell, J.A., Strazisar, A.J., and Seasholtz, R.G., "Efficient Laser Anemometer for Intra-Rotor Flow Mapping in Turbomachinery," ASME Journal of Engineering for Power, Vol. 103, No. 2, April 1981, pp. 424-429.

10. Ng, W.F., "Time-Resolved Stagnation Temperature Measurement in a Transonic Compressor Stage," MIT GTL Report No. 177, 1983, p. 20.

11. Holt, J.L., "Time-Resolved Flowfield Measurements in a Turbine Stage," MIT S.M. Thesis, 1985.

12. Figuerido, W.A., "Spherical Pressure Probe for Retrieving Freestream Pressure and Directional Data," MIT GTL Report No. 137, 1977.

13. Young, W.H., Meyers, J.F., and Hepner, T.E., "Laser Velocimeter Systems Analysis Applied to a Flow Survey Above a Stalled Wing," NASA TN D-8408, August 1977.

14. Lamb, H.L., Hydrodynamics, Dover, New York, 1945.

15. Chen, Y.F., "Fluctuating Lift Forces of the Karman Vortex Street on Single Circular Cylinders and in Tube Bundles Part 1," Journal of Engineering for Industry, May 1972.

16. Shaefer, J. and Eskinazi, S., "An Analysis of the Vortex Street Generated in a Viscous Fluid," Journal of Fluid Mechanics, Vol. 6, 1959.

17. Griffin, O. and Ramberg, S., "On Vortex Strength and Drag in Bluff-Body Wakes," Journal of Fluid Mechanics, Vol. 69, 1975.

18. Ng, W.G. and Epstein, A.H., "Unsteady Losses in Transonic Compressors," J. Eng. for Power, Vol. 107, No. 2, 1985.

19. Greenway, M.E. and Wood, C.J., "The Effect of a Bevelled Trailing Edge on Vortex Shedding and Vibration," _JFM_, Vol. 61, part 2, 1973.

20. M. Kurosaka, Private Communication.

21. Cumpsty, N.A. and Whitehead, D.S., "The Excitation of Acoustic Resonances By Vortex Shedding," _J. Sound Vib._, Vol. 18, No. 3, 1971.

22. Parker, R., "An Investigation of Acoustic Resonance Effects in an Axial Flow Compressor Stage," _J. Sound Vib._, Vol. 8, No. 2, 1968.

23. Camus, J.J. and Bryanston-Cross, P.J., "1 MHz Bandwidth, Real Time Schlieren Techniques in a Linear Cascade," _Proc. of Symposium Measurement Techniques in Transonic and Supersonic Flows in Cascades and Turbomachines_, Lyon, 1981.

Table 1 - Rotor Blade Vortex Street Parameters

Spacing Ratio (h/a)	= 0.635
Core-Radius Ratio (r_o/h)	= 0.50
Pressure-Defect Velocity Ratio (U_p/U_∞)	= 0.22
Vortex Strength ($k/[2*\pi*a*U_\infty]$)	= 0.07
Induced Velocity Ratio (U_i/U_∞)	=-0.21
Chen's Universal Wake, C	= 0.72
Vortex Shedding Frequency	= 16 kHz

Table 2 - Comparison of Vortex Model to LA Data

		LA Data	Vortex Model
Wake Depth	$1-(V_{cl}/U_\infty)$	0.126	0.088
Velocity Probability	(V/U_∞)high	1.18	1.17
Density Distribution	(V/U_∞)low	0.95	0.95
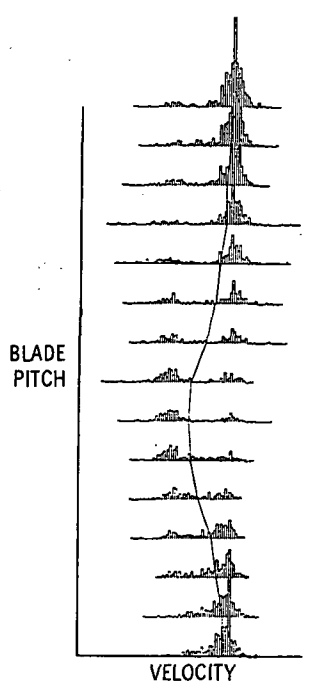
Fig. 1   Laser anemometer measurements showing mean velocity distribution and velocity histograms at each blade-to-blade measurement point.
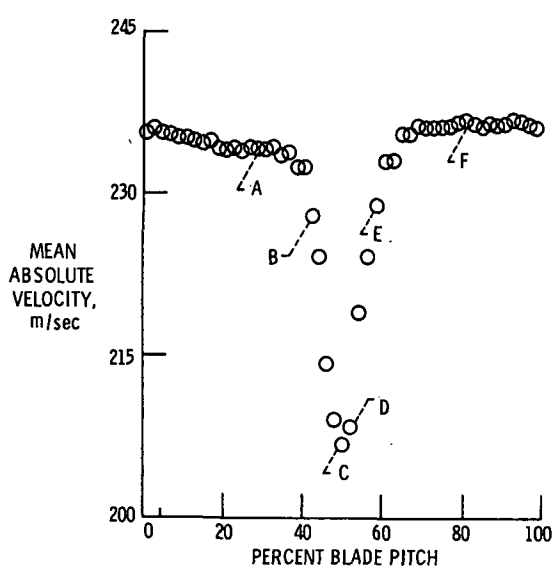
Fig. 2   Mean absolute velocity distribution measured by the LA at 60% span, 140% chord in a plane 42 degrees from the axial direction.

N/N_{max}

A V = 233 m/sec

F V = 236 m/sec

B V = 227 m/sec

E V = 228 m/sec

C V = 205 m/sec

D V = 207 m/sec

150   300   150   300

VELOCITY, m/sec
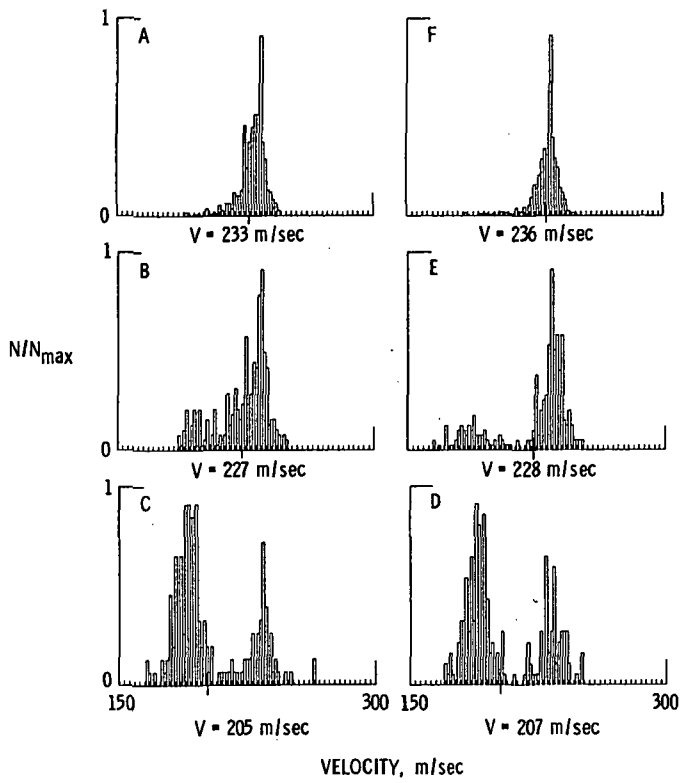
Fig. 3 Probability density distributions of velocity at points A-F in Figure 2.

ANGLE, deg

(a) Instantaneous.

(b) 90 rev averaged.

TIME, ms

Fig. 4 Relative flow angle at 140% chord measured with the ellipse probe.

VMEAS, m/sec

(a) Instantaneous.

(b) 90 Rev averaged.

TIME, ms

Fig. 5 Velocity component of probe measurement corresponding to LA measurement in Figure. 2.

N/N_{max}

A   F

B   E

C   D

120   330   120   330

VELOCITY, m/sec
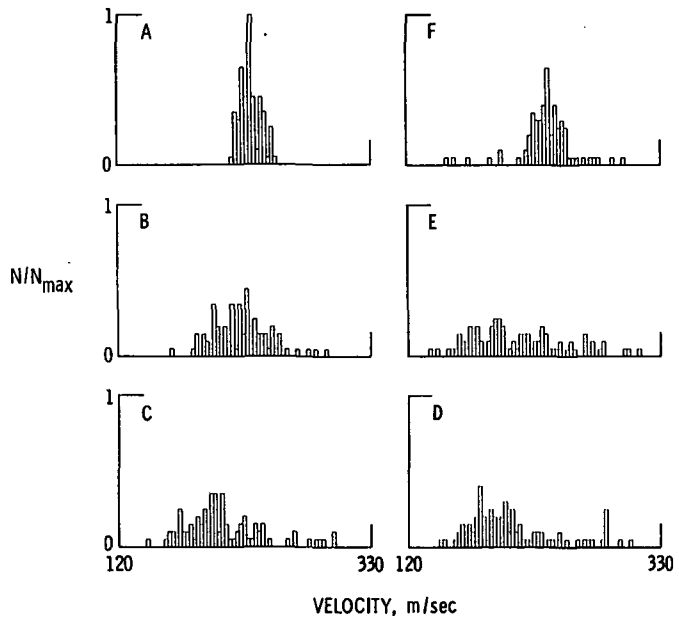
Fig. 6 Probability density distribution of component of probe measurement shown in Figure 5 at corresponding points.

9
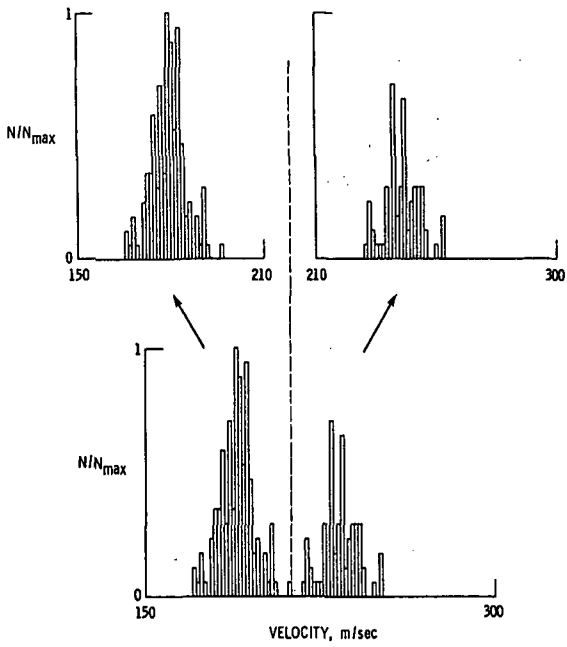
Fig. 7   Partitioning of bi-modal probability
         density distribution obtained in the wake.

Fig. 8   Distribution of mean absolute velocity as
         measured by LA, including effect of
         partitioning p.d.d.

Fig. 9   Geometry and nomenclature used in blade
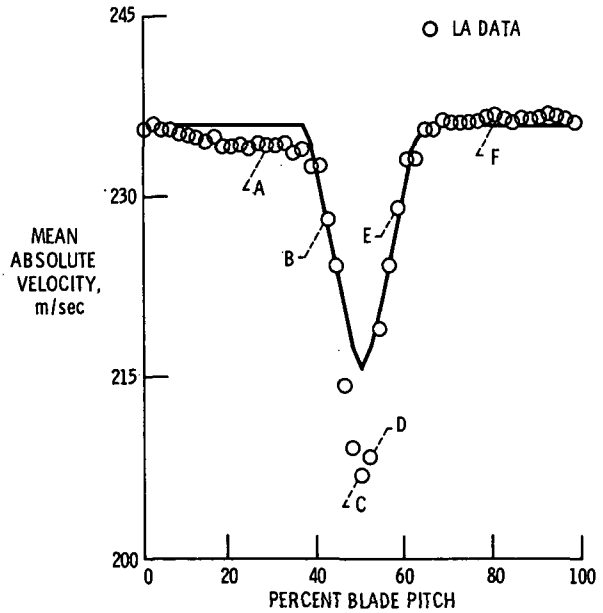   wake vortex model.

Fig. 10   Comparison of LA data from Figure 2 with
          wake model fit.

10
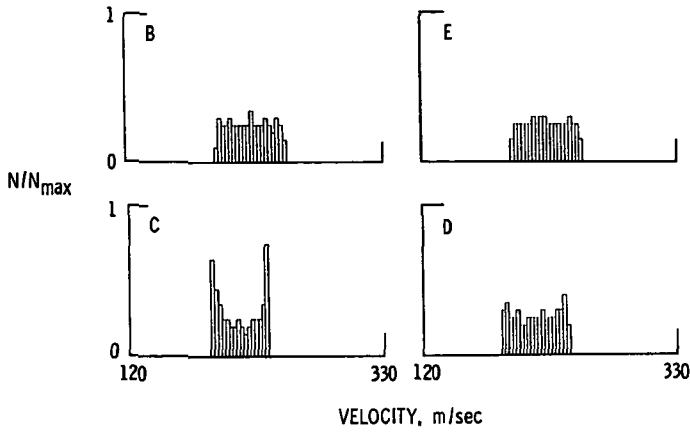
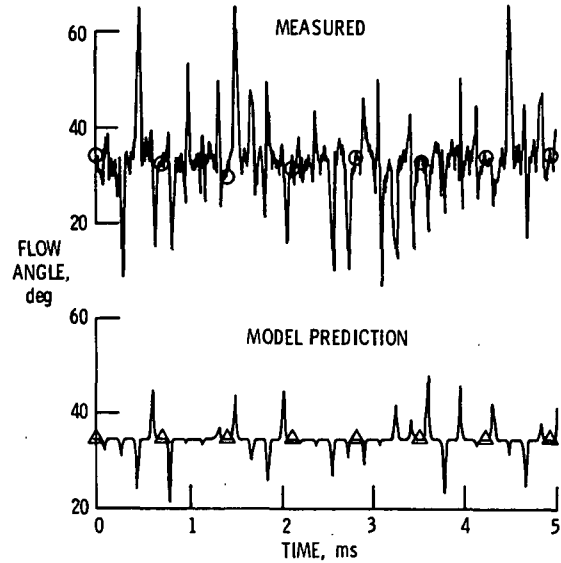Fig. 11   Probability density distributions from wake model.

Fig. 12   A comparison of rotor exit relative flow angle measured with ellipse probe to prediction by wake model.
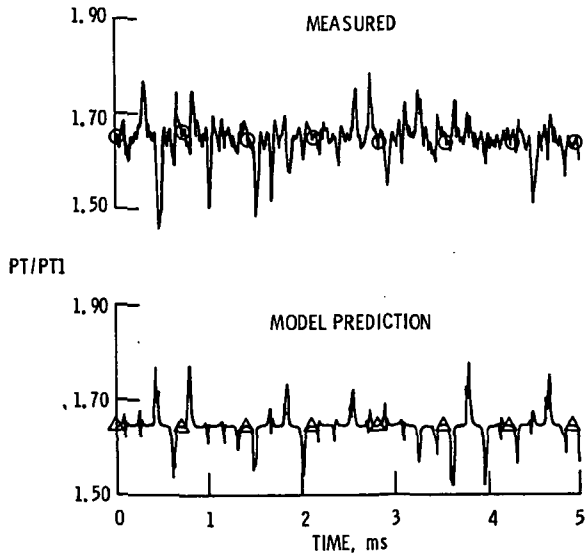

Fig. 13   Comparison of rotor total pressure ratio measured with ellipse probe to prediction by wake model.
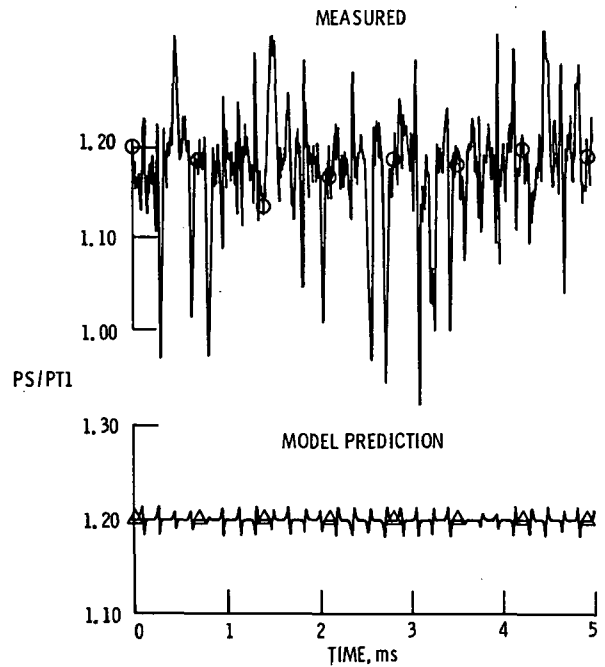

Fig. 14   Comparison of ratio of rotor exit static to upstream total pressure as measured by ellipse probe to wake model prediction.

11

070

1. Report No. NASA TM-87073 USAAVSCOM-TR-85-C-8 AIAA-85-1133	2. Government Accession No.	3. Recipient's Catalog No.
4. Title and Subtitle Rotor Wake Characteristics of a Transonic Axial Flow Fan		5. Report Date
		6. Performing Organization Code 505-31-04
7. Author(s) M.D. Hathaway, J. Gertz, A. Epstein, and A.J. Strazisar		8. Performing Organization Report No. E-2644
		10. Work Unit No.
9. Performing Organization Name and Address NASA Lewis Research Center and Propulsion Directorate, U.S. Army Aviation Research and Technology Activity- AVSCOM, Cleveland, Ohio 44135		11. Contract or Grant No.
		13. Type of Report and Period Covered Technical Memorandum
12. Sponsoring Agency Name and Address National Aeronautics and Space Administration Washington, D.C. 20546 and U.S. Army Aviation Systems Command, St. Louis, Mo. 63120		14. Sponsoring Agency Code

16. Abstract

State of the art turbomachinery flow analysis codes are not capable of predicting the viscous flow features within turbomachinery blade wakes. Until efficient 3D viscous flow analysis codes become a reality there is therefore a need for models which can describe the generation and transport of blade wakes and the mixing process within the wake. To address the need for experimental data to support the development of such models, high response pressure measurement and laser anemometer velocity measurements have been obtained in the wake of a transonic axial flow fan rotor.

17. Key Words (Suggested by Author(s)) Laser Doppler Velocimeter Vortex shedding Transonic compressor	18. Distribution Statement Unclassified - unlimited STAR Category 7		
19. Security Classif. (of this report) Unclassified	20. Security Classif. (of this page) Unclassified	21. No. of pages	22. Price*

National Aeronautics and
Space Administration

Lewis Research Center
Cleveland, Ohio 44135

Official Business
Penalty for Private Use $300

SECOND CLASS MAIL

ADDRESS CORRECTION REQUESTED

Postage and Fees Paid
National Aeronautics and
Space Administration
NASA-451

NASA